Bioresource Technology 426 (2025) 132329

Contents lists available at ScienceDirect

Bioresource Technology

journal homepage: www.elsevier.com/locate/biortech

Influence of vapothermal and hydrothermal pre-treatment on anaerobic degradability of lignocellulosic biomass

Jana Schultz [a,*], Marvin Scherzinger [a], Timo Steinbrecher [a], Asli Isci [b], Martin Kaltschmitt [a]

[a] Hamburg University of Technology (TUHH), Institute of Environmental Technology and Energy Economics (IUE), Eißendorfer Str. 40, 21073 Hamburg, Germany
[b] Ankara University, Food Engineering Department, 06830 Golbasi, Ankara, Turkey

HIGHLIGHTS

- Novel comparison of vapothermal and hydrothermal pre-treatment of lignocellulose.
- Vapothermal pre-treatment: improved AD at a biomass water content of 32–46 wt-%$_{FM}$.
- Both pre-treatments: altered structure and composition, incl. glucan retention.
- Increase of methane potential at 170 °C: 28 % (hydrothermal) and 36 % (vapothermal)
- Vapothermal pre-treatment: lower carbon loss, less energy requirements.

GRAPHICAL ABSTRACT

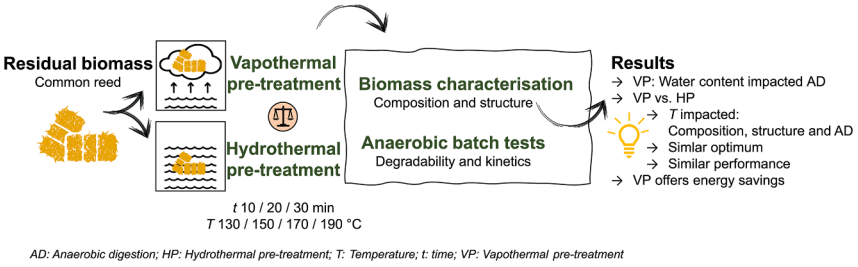

AD: Anaerobic digestion; HP: Hydrothermal pre-treatment; T: Temperature; t: time; VP: Vapothermal pre-treatment

ARTICLE INFO

Keywords:
Biomethane
Anaerobic digestion
Biomass valorization
Lignocellulose
Steam pre-treatment
Liquid hot water
Agricultural residues

ABSTRACT

This study compares the biogas potential of solid common reed residues after undergoing vapothermal and hydrothermal pre-treatment, accompanied by a compositional and structural biomass characterization. In a pre-test series, a design of experiments approach was used to determine the influence of the initial biomass water content during vapothermal pre-treatment on the biogas yield. In the main test series, common reed was pre-treated hydrothermally (i.e., in liquid water) and vapothermally (i.e., in saturated steam) while varying temperature and residence time. The initial biomass water content significantly impacted the biogas potential, with an optimum at a value of 32 to 46 wt–%$_{FM}$. In the main test series, unlike the residence time, temperature significantly impacted the subsequent anaerobic digestion. Vapothermal pre-treatment had a narrow temperature optimum while hydrothermal pre-treatment led to a biogas increase in a broader temperature range. The optimum temperature of both methods was 170 °C, where methane potentials increased by 28 % (vapothermal) and 36 % (hydrothermal) compared to the untreated sample. Considering the mass loss occurring during the pre-treatment, this increase was still 18 % for vapothermal pre-treatment, while it diminished the increase to 6 % for hydrothermal pre-treatment.

Overall, vapothermal pre-treatment produced a similar amount of biogas under comparable conditions, but was less susceptible to carbon loss, and, according to an estimation of the required process energy, may offer energy savings compared to hydrothermal pre-treatment.

* Corresponding author.
E-mail address: jana.schultz@tuhh.de (J. Schultz).

https://doi.org/10.1016/j.biortech.2025.132329
Received 17 December 2024; Received in revised form 7 February 2025; Accepted 1 March 2025
Available online 2 March 2025

1. Introduction

Residual lignocellulosic biomass from agriculture or industrial biomass processing is a largely untapped alternative to conventional energy crops as biogas substrate (IEA, 2020). Aiming to use these feedstocks for biogas production, reducing their inherent recalcitrance towards anaerobic digestion is essential to drive broader adoption. In this context, pre-treatment is seen as a crucial stage when it comes to biomass utilization (Ruiz et al., 2023). The term "pre-treatment" can be referred to as "a process step which converts lignocellulosic biomass from its native form, in which it is recalcitrant to cellulase enzyme systems, into a form for which enzymatic hydrolysis is effective" (Lynd et al., 2002). Accordingly, an effective pre-treatment should improve the accessibility of the fermentable building units of cellulose and hemicellulose often encapsulated in anaerobically non-degradable lignin structures. Further mechanisms for a successful pre-treatment are an increase of the surface area, a reduction of cellulose crystallinity – to allow enzymes to access cellulose monomers more easily – and a reduction in the sheathing of cellulose by hemicellulose (Baksi et al., 2023; Mosier et al., 2005). Biomass pre-treatment methods can be categorized into three major groups: physical, chemical, and biological pre-treatment. Methods combining two or more mechanisms can be referred to as physicochemical or biochemical pre-treatment (Agbor et al., 2011; Baksi et al., 2023).

Methods using hot water or steam are regarded as the most promising for biomass processing within biorefineries (Ruiz et al., 2023). This study therefore focuses on the two pre-treatment methods vapothermal and hydrothermal treatment. Both methods avoid the use of environmentally harmful chemicals and offer good scalability. Table 1 provides an overview of the main pre-treatment conditions, functioning mechanism, as well as the strengths and weaknesses of the two methods.

In vapothermal pre-treatment, also referred to as (uncatalyzed) steam treatment (Agbor et al., 2011; Mosier et al., 2005), biomass is treated using saturated steam at elevated pressure. The distinction from steam explosion pre-treatment is not always clear-cut (Olsson, 2007), because physical alterations caused by the "explosion" due to the sudden pressure release do not, or only weakly, contribute to the cellulose accessibility (Mosier et al., 2005). Hydrothermal pre-treatment also referred to as hot water pre-treatment, aquasolv, aqueous fractionation, and hydrothermolysis, involves the treatment of the biomass within liquid hot water (Agbor et al., 2011; Bisaria, 2024; Mosier et al., 2005). In the case of liquid hot water treatment pressure is applied at the same time to keep the water liquid (Mosier et al., 2005). Overall, the mode of action and the effect of vapothermal and hydrothermal pre-treatment are relatively similar, involving hemicellulose (auto-)hydrolysis and solubilization, as well as lignin disintegration and dissolution, while retaining cellulose within the solid fraction in a more accessible form. Due to limited literature on pure vapothermal/steam pre-treatment of lignocellulosic biomass, steam explosion studies were included in the discussion, since the effects of the treatments are similar (Olsson, 2007). Also, literature on liquid hot water pre-treatment was taken into consideration for evaluating the hydrothermal pre-treatment.

Comparisons of both methods are available for enzymatic hydrolysis and subsequent bioethanol production (Perez-Cantu et al., 2013), as well as carbonization (Funke et al., 2013). In the case of bioethanol production, it was shown that both methods yielded relatively similar results (Perez-Cantu et al., 2013). However, vapothermal pre-treatment may offer advantages in terms of energy efficiency because less water needs to be heated, (Funke et al., 2013), shorter residence times are effective (Ferreira et al., 2013) and less carbon is lost to the liquid fraction during the pre-treatment (Funke et al., 2013). Nevertheless, pre-treatment requirements for biogas production may differ from those for bioethanol production and carbonization, and direct comparisons of both methods for lignocellulosic biomass pre-treatment and subsequent biogas production are scarce.

Against this background, this paper assesses vapothermal and hydrothermal pre-treatment under comparable pre-treatment conditions, namely pre-treatment temperature and residence time. For evaluating the effectiveness of the methods, biogas and methane potentials as well as compositional and structural characteristics of the solid residues and the mass loss occurring during pre-treatment were determined. In addition, the evaluation is supported by an estimation of the energy demand for the respective processes. A pre-test series was conducted to optimize the biomass water content via water impregnation prior to vapothermal pre-treatment, because it can impact the pre-treatment performance greatly (Parsin and Kaltschmitt, 2024), e.g., by enabling a better heat transfer (Sui and Chen, 2016).

2. Materials and methods

2.1. Procedure

The procedure and scope of analysis are presented in Fig. 1. The investigation was divided into two experimental series. In the pre-test series, the influence of pre-treatment parameters during vapothermal pre-treatment (i.e., pre-treatment temperature, residence time, and initial biomass water content) on the biogas potential of the solid process residues was investigated. Emphasis was put on the initial biomass water content. In the main test series, vapothermal (using the optimized initial water content) and hydrothermal pre-treatment were conducted under the same pre-treatment conditions. The overall scope of the investigation was restricted to the remaining solid residues of the pre-treated biomass, as these are considered process residues with potential for energy production via anaerobic digestion. The liquid phase was excluded from the analysis because it could be valorized through other pathways beyond the focus of this study.

2.1.1. Pre-test series: Influence of the biomass water content during vapothermal pre-treatment

For the pre-test series, a 3-level, 3-factor Box-Behnken design was employed to investigate major effects as well as interaction and quadratic effects of the three pre-treatment factors pre-treatment

Table 1
Overview of vapothermal and hydrothermal pre-treatment (Agbor et al., 2011; Bisaria, 2024; Mosier et al., 2005; Wang et al., 2023).

	Vapothermal pre-treatment	Hydrothermal pre-treatment
Medium	Saturated steam at elevated pressure	Hot water at elevated pressure
Temperature	160 – 260 °C	100 – 230 °C
Residence time	s to min	min to h
Mechanism	Autohydrolysis and dissolution of hemicellulose components, autoprotolysis of water, biomass/lignin disintegration	Autohydrolysis and dissolution of hemicellulose components, autoprotolysis of water, biomass/lignin disintegration
Substrates	Agricultural, lignocellulosic residues, grass cuttings, municipal solid waste, hard- and softwood	Agricultural, lignocellulosic residues, grass cuttings, municipal solid waste
Strengths	Low corrosion, no chemical consumption, low water consumption, low energy consumption, low organic matter loss	Low corrosion, no chemical consumption, low formation of inhibitors
Weaknesses	Formation of inhibitors	High water consumption, high energy consumption, high organic matter loss, high amounts of wastewater

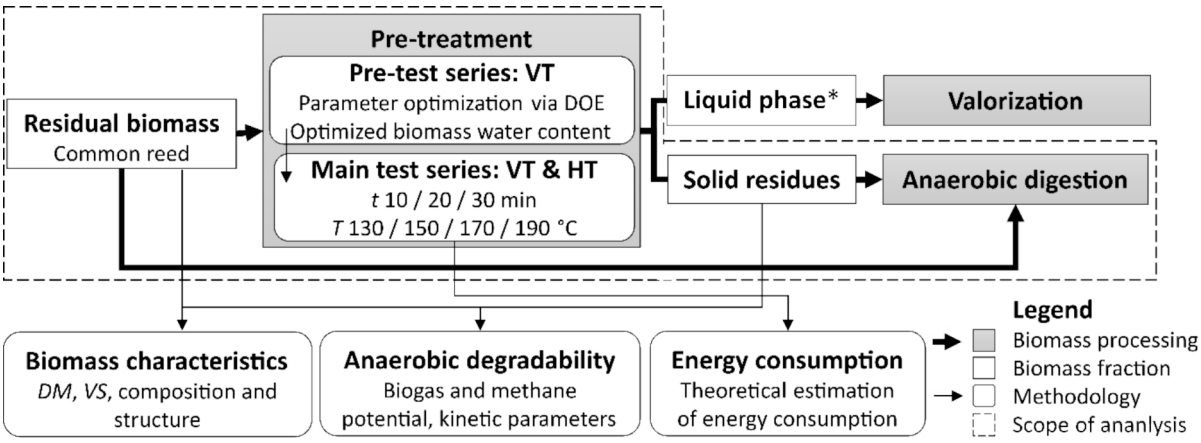

Fig. 1. Procedure and scope of analysis. VT: Vapothermal pre-treatment; HT: Hydrothermal pre-treatment; DOE: design of experiments; *t*: time; *T*: Temperature; *DM*: Dry mass; *VS*: Volatile solids. *Liquid at standard conditions.

Table 2
Pre-test series: varied pre-treatment factors, symbols, and coded levels in the Box-Behnken design.

Factor	Symbol	Coded level		
		−1	0	+1
Temperature (°C)	*A*	130	155	180
Time (min)	*B*	30	60	90
Water content (wt-%$_{FM}$)	*C*	7.4	33.7	60.0

temperature, residence time, and initial biomass water content. It involved the variation of all factors on a lower, a medium, and a higher level (coded levels in Table 2). In each experimental run, two factors were varied across the three levels while the third factor was kept at the medium level (Siebertz et al., 2017). The center point was investigated four times to estimate the pure error. The lowest factor level of the water content was set to the initial biomass water content before water impregnation (7.4 wt–%$_{FM}$). The upper limit was set to the maximum amount of water the biomass could take up (60 wt–%$_{FM}$).

The impact of the parameters was evaluated by establishing a mathematical relationship between the factors *A*, *B,* and *C* as independent variables and the biogas potential (Y_M) as the dependent variable (response variable). A regression model was fitted to the data, specifically, the relationship was expressed using a second-degree quadratic polynomial function (equation (1)).

$$Y_M = \beta_0 + \beta_1 A + \beta_2 B + \beta_3 C + \beta_{11} AB + \beta_{12} AC + \beta_{13} BC + \beta_{21} A^2 + \beta_{22} B^2 + \beta_{23} C^2 \quad (1)$$

β_0 is the intercept coefficient, the other coefficients are linear coefficients (β_1, β_2, β_3), interaction coefficients (β_{11}, β_{12}, β_{13}), and quadratic coefficients (β_{21}, β_{22}, β_{23}) (Scherzinger et al., 2020).

To evaluate the acceptability and significance of the model, it was evaluated through an analysis of variance (ANOVA) and a regression analysis, as well as the following descriptive statistics: the *F*-value, the coefficient of determination (R^2), the adjusted coefficient of determination (R^2_{adj}), and the predicted coefficient of determination (R^2_{pred}) (Buratti et al., 2018). The confidence level was $\alpha = 0.05$. Based on the fitted model, a response surface plot was generated, visualizing the influence of the parameters on the biogas potential. The response surface plot was created by selecting parameters of interest that demonstrated a significant effect.

2.1.2. Main test series: Comparison of the solid products of vapothermal and hydrothermal pre-treatment

The experimental plan for the main test series (Fig. 1), specifically the comparison of the biogas and methane potential from the solid products remaining after vapothermal and hydrothermal pre-treatment, was based on the pre-test series. Accordingly, the biomass water content during vapothermal pre-treatment was kept at 35 wt–%$_{FM}$ for all experiments without variation. Since the residence time had the least effect within the pre-test series, the pre-treatment time was varied in a lower range thereafter (i.e., 10, 20, and 30 min, all 150 °C). The parameter variation of the pre-treatment temperature was conducted at four levels (i.e., 130, 150, 170, and 190 °C, all 30 min).

2.2. Substrate

Common reed harvested from a large constructed wetland for the treatment of wastewater from oil production located in Oman was used as lignocellulosic substrate. It was sundried, coarsely shredded, and homogenized via fractional shoveling (Pitard, 1993) and reunifying fractions randomly afterward. The characteristics of the untreated substrate are presented in Table 3.

2.3. Pre-treatment

2.3.1. Vapothermal pre-treatment

For the vapothermal pre-treatment, to adjust the water content of the common reed according to the experimental plan, 100 g of common reed was added to a bucket with the respective amount of tap water and mixed in an overhead shaker for at least 60 min. It was then filled into a metal basket placed inside a rotation reactor ($V = 65$ L, custom-built, Estanit, Germany). The metal basket was fitted with a stainless-steel mesh (mesh size 200) to avoid material loss and to avoid direct contact with the heated reactor surface and the water inside the reactor. 1 L of tap water was added to the reactor to provide water to form water vapor. The reactor was closed and heated up to the respective temperature until the saturation pressure was reached and kept constant for the

Table 3
Characteristics of substrate and inoculum used in the present study. NA: not available.

Parameter	Substrate	Inoculum	
	Common reed	Pre-test series	Main test series
DM (%$_{FM}$)[a]	92.84 ± 0.11	2.48 ± 0.01	1.99 ± 0.01
VS (%$_{DM}$)[a]	93.05 ± 0.13	62.94 ± 0.19	61.28 ± 0.24
Cellulose (%$_{DM}$)[b]	39.9 ± 0.3	NA	NA
Hemicellulose (%$_{DM}$)[b]	23.6 ± 0.0	NA	NA
Lignin (%$_{DM}$)[b]	22.9 ± 0.5	NA	NA

[a] $n = 3$.
[b] $n = 2$.

specified residence time (procedure, section 2.1) was reached and kept constant for the specified residence time. The reaction was stopped by slowly releasing the steam from the reactor.

2.3.2. Hydrothermal pre-treatment

For the hydrothermal pre-treatment, 30 g of common reed was mixed with 300 mL water (1:10 solid-to-solvent ratio). The pre-treatment was conducted in a Parr Reactor (Model 4520, Parr, USA) at temperatures and residence times as specified by the experimental plan (procedure, section 2.1). The slurry was constantly mixed at a speed of 150 min^{-1}. After the pre-treatment, the solids were vacuum-filtered and washed with 250 mL of water.

2.4. Biomass characterization and biogas potential

After pre-treatment, the biomass was dried at 45 °C overnight and milled below 1 mm particle size using a cutting mill (MF 10, IKA, Germany) in preparation for the subsequent analysis.

2.4.1. Dry mass and volatile solids content

The dry mass and volatile solids content of the biomass samples were determined according to DIN methods (DIN EN ISO 18134, 2015) and (DIN EN 15935, 2012), respectively. Drying was performed in an oven (U80, Memmert, Germany), and incineration in a muffle furnace (M104, Thermo Scientific Heraeus, USA; for results see supplementary).

2.4.2. Mass loss

The mass loss (ML_v) of the samples after vapothermal pre-treatment was estimated based on the ash content of the dry sample before (c_a) and after pre-treatment ($c_{a,t}$) (equation (2)), assuming that the ash was not removed from the biomass due to pre-treatment (Lizasoain et al., 2016). A gravimetric method was not possible here due to the partial adhering of biomass on the mesh.

$$ML_v = ((c_{a,t} - c_a)/c_{a,t})100\% \quad (2)$$

The mass loss (ML_h) of the samples due to hydrothermal pre-treatment was determined gravimetrically and calculated from the dry mass of the sample before (m_d) and after pre-treatment ($m_{d,t}$, equation (3)).

$$ML_h = (1 - m_{d,t}/m_d)100\% \quad (3)$$

2.4.3. Biogas and methane potential and determination of kinetic parameters

The biogas potential of the common reed samples was determined in batch mode under mesophilic conditions (i.e., 37 ± 1 °C) (Verein Deutscher Ingenieure, 2016). As inoculum, 400 mL sewage sludge (wastewater treatment plant Seevetal, Germany, characteristics provided in Table 3) was filled into 500 mL reactors and connected to eudiometer tubes filled with a sealing liquid allowing to determine the biogas volume. The inoculum was outgassed for at least 7 d. 2.5 g_{VS} of the solid pre-treatment residues were added to the reactors and the reactors' headspaces were purged with N_2. Daily, the produced biogas volume V was determined by reading the level change of the sealing liquid. Ambient pressure and temperature were noted and reactors were mixed using a magnetic stirrer. The experimental duration was 46 to 48 d, depending on when the daily biogas production undershot a production of 0.5 % of the total biogas production for 3 d in a row. The biogas volume of dry gas at standard conditions $V_{dry,N}$ was calculated according to equation (4).

$$V_{dry,N} = V\frac{(p - p_w)T_N}{p_N T} \quad (4)$$

p is the ambient pressure, p_w the water vapor pressure derived from the Magnus formula, p_N the normal pressure (p_N = 1,013 hPa), T_N the normal temperature (T_N = 273 K), and T the ambient temperature.

The biogas potential (biogas yield) Y_{BG} of the samples was then determined by referring the volume $V_{dry,N}$ to the organic dry mass $m_{d,org}$ given into the reactors (equation (5)).

$$Y_{BG} = V_{dry,N}/m_{d,org} \quad (5)$$

The biogas potential $Y_{BG/DOM}$ based on the digestible organic dry mass, here defined as all organic mass besides lignin, was calculated by considering the mass-based lignin content x_{lig} and ash content x_a according to equation (6).

$$Y_{BG/DOM} = Y_{BG}\frac{(1 - x_a)}{(1 - x_a - x_{lig})} \quad (6)$$

The CH_4 and CO_2 content of the biogas was measured with a portable gas analyzer (Biogas 5000, Geotech, UK). The methane potential was calculated under the assumption that the dry gas in normal state consists of CH_4 and CO_2 only. Experiments were determined in triplicates.

The Tukey post hoc test was used to assess the statistical difference between values at a level of significance of $\alpha = 0.05$.

The kinetic parameters of the anaerobic degradation were calculated using the Modified Gompertz Model (Velázquez-Martí et al., 2019) shown in equation (7).

$$P = P_0 exp\left[- exp\left(\frac{R_m e}{P_o}(t - \lambda) + 1\right)\right] \quad (7)$$

The cumulative biogas production P at time t was calculated from the maximum biogas yield P_0, the maximum biogas rate R_m, with the lag phase λ and the Euler's number e (e = 2.7182).

2.4.4. Compositional analysis

The structural carbohydrates and lignin in the solid biomass were determined according to the respective NREL procedure (Sluiter et al., 2008). This analysis involved a two-step hydrolysis to fractionate and dissolve the carbohydrates. The concentration of the dissolved sugars (i.e., D-cellobiose (CAS 528–50-7), D(+)glucose (CAS 50-99-7), D(+)xylose (CAS 58-86-6), L(+)arabinose (CAS 147-81-9)) and acetic acid (CAS 64-19-7) was measured with an HPLC system (1260 Infinity II, Hi-Plex H + column, refraction index detector (all Agilent, USA), eluent: 5 mM sulfuric acid (CAS 7664-93-9, Carl Roth)). The glucan (corresponding to the cellulose content hereafter), arabinoxylan (corresponding to the hemicellulose content hereafter), and acetate contents of the original samples were calculated as specified in (Sluiter et al., 2008). Acid-soluble lignin was determined by UV spectrometry (Cary 50 Bio, Varian, USA) using a wavelength of 320 nm and an absorptivity of 30 L g^{-1} cm^{-1}. Insoluble-lignin was determined by subtracting the ash content from the insoluble solids remaining after the hydrolysis (Sluiter et al., 2008). The total lignin was calculated as the sum of both. Measurements were carried out in duplicates.

2.4.5. Structural analysis

For structural analysis, Fourier-transformation infrared spectrophotometry (FTIR) spectra were measured using a Vertex 70 spectrometer (Bruker Optik, Germany) equipped with a single bounce diamond attenuated total reflectance (ATR) insert (MIRacle, Pike Technologies, USA). A liquid-cooled mercury cadmium telluride (MCT) detector was used for the recording of the spectra. Before the measurement, the instrument was purged with dry, carbon-free air. The measurement range was set to 4,000 to 600 cm^{-1}, recording 64 scans per spectrum. Spectra recording, as well as data processing (baseline correction and peak integration), was performed using OPUS (OPUS 7.0, Bruker, Germany).

To evaluate the spectra with regard to structural and compositional information, different indices were calculated. Specifically, the crystallinity ratio (*CR*) and the lateral order index (*LOI*), which were measured to assess structural changes, as well as the cellulose-to-lignin ratio (*CL*), were determined according to the equations (8), (9), and (10).

$$CR = a_{1,372}/a_{2,900} \quad (8)$$

$$LOI = a_{1,437}/a_{898} \quad (9)$$

$$CL = (a_{1,425} + a_{1,160})/a_{1,515} \quad (10)$$

a is the absorbance at the wavenumber as specified in the subscript.

The *CR* decreases with decreasing crystallinity and vice versa. Crystallinity changes rather affect the peak at 1,372 cm^{-1} (C—H bending), while the peak around 2,900 cm^{-1} is usually not affected (C—H stretching in CH_2 group, peak maximum here: 2,926 cm^{-1}) (Nelson and O'Connor, 1964).

An increasing *LOI* may indicate increasing crystallinity of cellulose type I or decreasing crystallinity of cellulose type II (Nelson and O'Connor, 1964). An increasing *LOI* must not always be related to changes in crystallinity but might also be an indication of the transformation of cellulose type I to cellulose type II (Hurtubise and Krassig, 1960). The peak at 1,437 cm^{-1} (here peak maximum was at 1,425 cm^{-1}) is sensitive to allomorphic transformations or decrystallization. The peak at 898 cm^{-1} is usually not affected by changes in conformation (Lourdin et al., 2016). Similar to the *CR*, the *LOI* is proposed as a measure of cellulose crystallinity. At the same time, it is also affected by allomorphic transformation of cellulose type I (native cellulose) to cellulose type II (regenerated cellulose) (Hurtubise and Krassig, 1960).

The *CL* is based on the peaks at 1,425, 1,160, and 1,515 cm^{-1}. The 1,425 cm^{-1} peak is an indication of native cellulose (type I) (Lynam et al., 2017), the peak at 1,160 cm^{-1} is caused by amorphous cellulose (type I and type II) (Shi and Li, 2012), and the peak at 1,515 cm^{-1} shows the presence of lignin (Lynam et al., 2017).

2.5. Estimation of the energy demand

An estimation of the energy demand of both methods was carried out to facilitate evaluation. The calculation was restricted to the energy required to heat fresh biomass and treatment medium (i.e., steam and water) without considering periphery such as process machineries and their respective efficiencies or associated heat losses.

It was assumed that processing is carried out in batch mode being an adiabatic process. The biomass is introduced into the system at standard conditions. Accordingly, the starting temperature was set to 20 °C and the final temperature was 170 °C (i.e., the experimental optimum). The determination of the required energy was calculated as the total heat flow composed of the following terms: The energy needed for heating the biomass (dry mass) to process temperature was derived from the heat capacity of common reed ($c_{reed} = 1.2$ kJ kg^{-1} K^{-1} (FNR, 2024)). The energy required for heating water inside the biomass to 100 °C was calculated based on the heat capacity of water ($c_{water} = 4.2$ kJ kg^{-1} K^{-1}). For vapothermal pre-treatment, a biomass water content of 35 $\%_{FM}$ was assumed. The biomass water content for hydrothermal pre-treatment (including the treatment medium) was set to 90 $\%_{FM}$ resulting from a 1:10 solid-to-solvent ratio during pre-treatment. The heating of bulk water and steam from 100 °C to process temperature was calculated based on the heat capacity of water (boiling liquid, $c_{water,sat} = 4.4$ kJ kg^{-1} K^{-1}) and saturated steam ($c_{steam} = 2.6$ kJ kg^{-1} K^{-1}), respectively. The amount of steam needed to supply saturated steam at the given conditions was derived from the ideal gas law. The energy required to produce this amount of steam for vapothermal pre-treatment was calculated from the enthalpy of evaporation of water ($\Delta H_{vap,water}$ - = 2,257.4 kJ kg_{-1}). In the case of vapothermal pre-treatment, this steam is supplied externally, in the case of hydrothermal pre-treatment this term accounts for the evaporation of water in the closed system during the heating until a saturation state is reached.

3. Results and discussion

3.1. Pre-test series: Effect of water content during vapothermal pre-treatment

The coded model equation (coded factors as specified in equation (1)) for determining the biogas production yield (Y_M) from the varied pre-treatment conditions (*A*: temperature, *B*: residence time, *C*: water content) is shown in equation (11).

$$Y_M = +327.30 - 4.65A - 8.43B + 26.45C + 21.93AB + 46.12AC + 25.28BC - 52.16A^2 - 28.66B^2 - 65.96C^2 \quad (11)$$

Table 4 provides the ANOVA of the generated model and experimental data. The *F*-value of the model of 13.38 implies the model is significant, which is confirmed by the *p*-value of 0.0025 (*p*-values of < 0.05 indicate significance). The lack of fit *F*-value of 0.58 indicates non-significance relative to the pure error being in favor of the model. According to the model (column "*p*-value", Table 4) biogas production is significantly impacted by the water content (factor *C*), the interaction of temperature and water content (*A C*), the residence time and the water content (*B C*), as well as the squared factors of all factors (A^2, B^2, and C^2). The residence time and temperature themselves do not have a significant impact on the biogas yield.

Looking at the relationship between pre-treatment temperature and water content the biogas production (Y_m) was highest around a medium temperature and water content (Fig. 2A). The optimum parameters determined by the model were a pre-treatment temperature of 149 to 163 °C, a residence time of 47 to 71 min, and a water content of 32 to 46 wt–$\%_{FM}$ (tolerance of 5 mL_N g_{VS}^{-1} from the maximum of 330.1 mL_N g_{VS}^{-1}). The closest parameter setting investigated in the respective experimental trial were the four center points (155 °C / 60 min / 33.7 wt–$\%_{FM}$). The methane production resulting from this pre-treatment was 207.5 ± 16.4 mL_N CH_4 g_{VS}^{-1} (biogas potential 328.0 ± 21.1 mL_N g_{VS}^{-1}). Even though these pre-treatment conditions resulted in a higher biogas and methane potential compared to all other pre-treatment conditions, the biogas production did not differ significantly from the original untreated sample with a total methane potential of 195.4 ± 3.3 mL_N CH_4 g_{VS}^{-1} (biogas potential 309.6 ± 9.6 mL_N g_{VS}^{-1}). Hence, the pre-treatment did not improve the overall biogas potential at the given conditions.

Nevertheless, the pre-treatment affected the degradation kinetics of the reed. This is visible in the cumulative biogas production over time (Fig. 2B). Biomass degradation was faster at the beginning of the experiments, while the untreated sample had a longer lag phase and a relatively steady biogas production throughout the experiment. This observation is supported by the kinetic parameters (Table 5), as treated samples (155 °C / 60 min / 33.7 wt–$\%_{FM}$) had a much lower lag phase (λ) and a higher maximum biogas rate (R_m) compared to the original

Table 4
ANOVA of the quadratic responds surface model for determining the biogas production.

Source	Degrees of freedom	*F*-value	*p*-value
Model	9	13.3800	0.0025
A (Temperature)	1	0.4091	0.5461
B (Residence time)	1	1.3400	0.2905
C (Water content)	1	13.2400	0.0109
A B	1	4.5500	0.0769
A C	1	20.1300	0.0042
B C	1	6.0400	0.0492
A^2	1	25.7400	0.0023
B^2	1	7.7700	0.0317
C^2	1	41.1600	0.0007
Lack of fit	3	2.0000	0.2924
Pure Error	3		

$R^2 = 0.9525$, $R^2_{adj} = 0.8813$, $R^2_{pred} = 0.4658$.

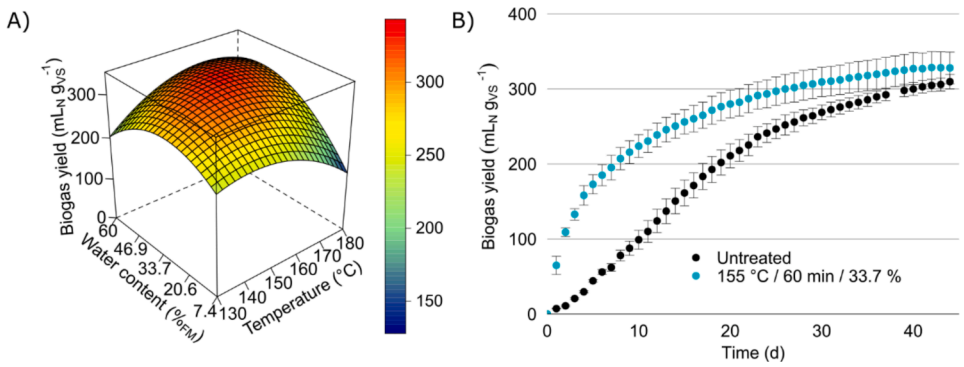

Fig. 2. A) Response surface plot of biogas production as a function of water content and temperature at a residence time of 60 min (factor B = 0). B) Biogas yield of untreated and vapothermal treated common reed over time (n = 3).

Table 5
Kinetic parameters of common reed after vapothermal pre-treatment (pre-test series). *T* Temperature, *t* residence time, *WC* water content, *P* cumulative biogas production, R_m biogas rate, λ lag phase, R^2 Coefficient of determination, *RMSE* root mean square error.

Treatment			P (mL$_N$ g$_{VS}^{-1}$)	R_m (mL$_N$ g$_{VS}^{-1}$ d^{-1})	λ (d)	R^2 (−)	RMSE (mL$_N$ g$_{VS}^{-1}$)
Untreated			310.8	12.41	2	0.999	3.64
T (°C)	t (min)	WC (wt–%$_{FM}$)					
130	30	33.7	251.9	12.63	2.0	0.998	3.55
130	60	7.4	244.8	10.77	0.2	0.996	4.52
130	60	60.0	207.6	10.53	0.3	0.994	4.69
130	90	33.7	200.4	11.61	0.1	0.997	3.44
155	30	7.4	229.0	11.14	−3.4	0.976	8.81
155	30	60.0	233.1	10.94	−1.5	0.992	5.90
155	60	33.7	317.6	16.60	−4.1	0.958	14.59
155	90	7.4	168.1	9.90	−4.8	0.879	11.75
155	90	60.0	276.9	18.36	−2.1	0.977	10.28
180	30	33.7	244.9	18.63	−0.9	0.993	5.44
180	60	7.4	101.2	5.37	−3.5	0.965	4.44
180	60	60.0	267.6	32.53	1.7	0.999	2.15
180	90	33.7	279.5	15.79	−0.2	0.995	6.01

sample.

The methane potential of untreated common reed (195.4 ± 3.3 mL$_N$ CH$_4$ g$_{VS}^{-1}$) measured in this study was slightly higher than the typically reported range of 100 to 150 mL$_N$ CH$_4$ g$_{VS}^{-1}$ (Baute et al., 2018; Roj-Rojewski et al., 2019). A certain deviation is expected, as the biomass characteristics and thus the biogas potential depend on many factors such as the growing conditions, harvest time, and plant age (Baute et al., 2018; Roj-Rojewski et al., 2019).

Since a detailed analysis of pre-treatment temperature and residence time will follow evaluating the main test series, this discussion focuses on the impact of initial biomass water content on anaerobic degradability. Actually, among the three factors investigated, water content had the strongest effect on biogas production, even though the overall biogas potential did not increase significantly. This observation is not generally supported by other investigations. For example, Ferreira et al. observed only a minor effect of adapting the initial water content prior to steam explosion (200 °C, 5 min) on the methane potential of wheat straw (Ferreira et al., 2014). Similarly, Wang et al. also applied a Box-Behnken design to investigate the anaerobic digestibility of bulbrush (Wang et al., 2010). According to their derived model, the optimized water content was 11 wt–%$_{FM}$ (range: 10 to 30 wt–%$_{FM}$), but among the three factors investigated only steam pressure, and residence time were significant predictors of the methane potential (Wang et al., 2010). In other application contexts, there is evidence that the performance of vapothermal or steam explosion pre-treatment may profit from an optimized water content. For instance, the initial water content of corn stalks was optimized during steam explosion pre-treatment as a compromise between pre-treatment efficacy – in terms of glucose yield after follow-up enzymatic hydrolysis – and energy efficiency (Sui and Chen, 2015). Treating the biomass at an initial water content of 40 wt–%$_{FM}$ resulted in a 20 % improved hydrolysis yield after pre-treatment and offered energy savings at the same time (Sui and Chen, 2015). Within another study an optimized water content led to a higher hemicellulose solubilization in the liquid hydrolysate after vapothermal pre-treatment (Parsin and Kaltschmitt, 2024). For that specific application – aiming to maximize hemicellulose solubilization while retaining the cellulose and lignin in the solid biomass – a water content of 50 wt–%$_{FM}$ was desirable (Parsin and Kaltschmitt, 2024). The optimum for the present application – biogas production – may differ from the reported finding, since removing the anaerobically degradable hemicellulose fully from the feedstock biomass is not necessarily an advantage for anaerobic digestion.

A possible underlying mechanism determining the pre-treatment success could be the presence of different states of water in the lignocellulosic biomass: the water bound inside the cell walls, the bulk water outside the cell walls, and the steam itself (Ziegler-Devin et al., 2021). A saturation of the cell wall-bound water of the lignocellulosic biomass is desirable. This water acts as a plasticizer, reducing the mechanical strength of the cell walls and enabling better heat transfer (Sui and Chen, 2016). The positive effect is related to biomass swelling by integrating cell-bound water, enlarging the pore sizes, and allowing steam to penetrate deeper into the lignocellulosic structures (Sui and Chen, 2016). Beyond the water saturation point, additional water will add up to the bulk water and hinder an effective steam penetration and heat transfer and eventually – as observed at higher water contents – diminish the pre-treatment effectiveness and increase energy consumption (Sui and Chen, 2016). Thus, the water content of the biomass needs to be adjusted until the cell wall water reservoir is saturated (Sui and Chen, 2016). In the present case, water needs to be added to the common reed until a water content of around 35 wt–%$_{FM}$ is reached. In

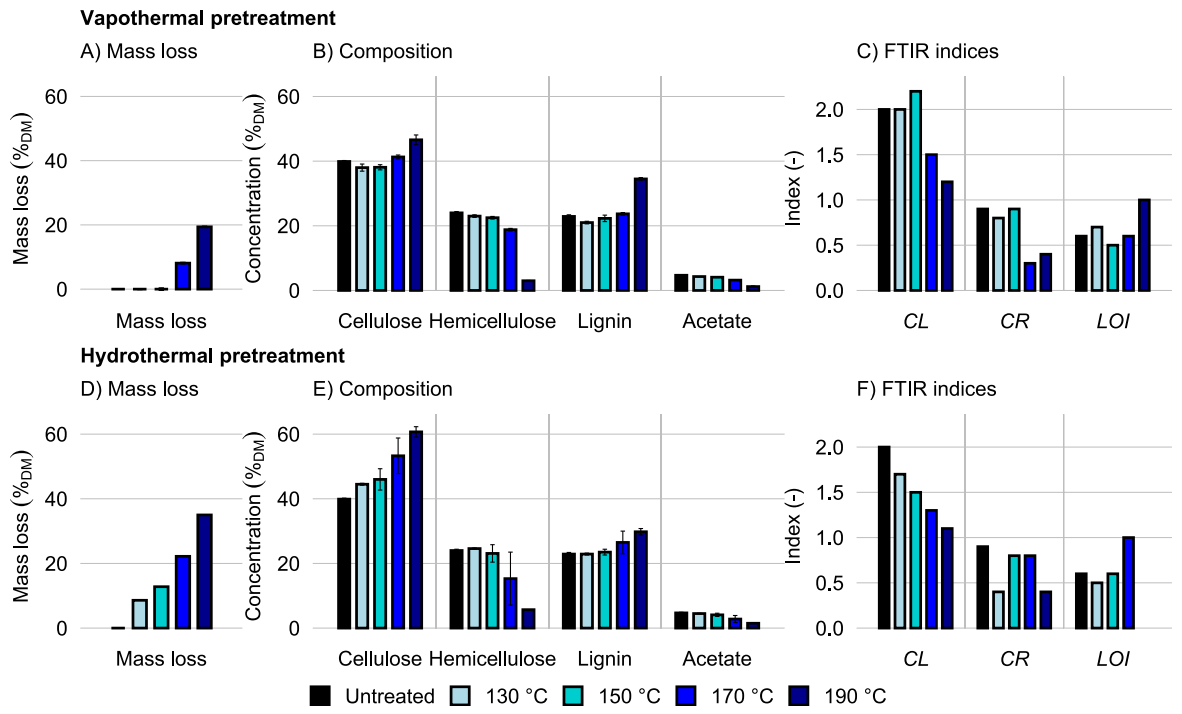

Fig. 3. Mass loss (A, D, (n = 3)), Composition (B, E, (n = 2)), and FTIR indices (C, F) after vapothermal pre-treatment (top) and hydrothermal pre-treatment (bottom). Residence time: 30 min. For one hydrothermally pre-treated sample (190 °C) it was not possible to determine the *LOI* as the integration of the respective peak was not possible. Error bars are not available for C, D, and F as no triple-determination was conducted.

certain circumstances, this influencing parameter could be a decisive factor for the effectiveness of the vapothermal pre-treatment when being compared to, e.g., hydrothermal pre-treatment, as it was done in the main test series of the present study.

3.2. Main test series: Comparison of solid products from vapothermal and hydrothermal pre-treatment

3.2.1. Mass loss and biomass composition

The mass loss caused by the pre-treatment differed considerably among the pre-treatment methods and was strongly impacted by

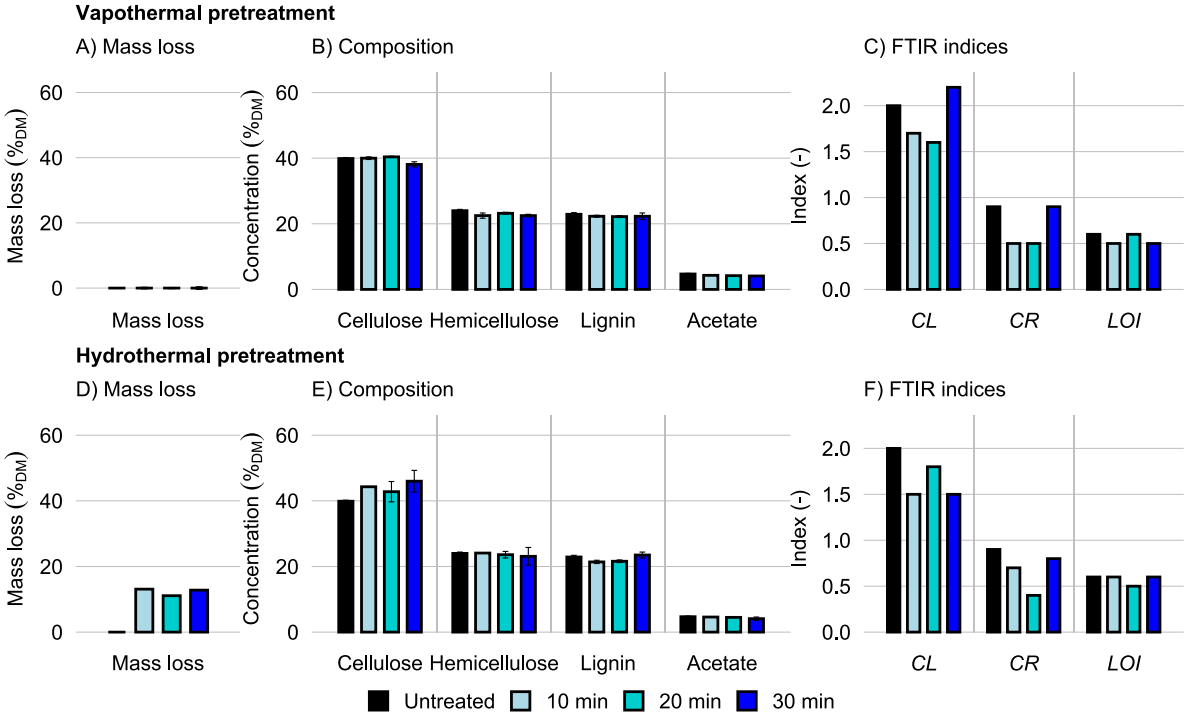

Fig. 4. Mass loss (A, D, (n = 3)), Composition (B, E, (n = 2), and FTIR indices (C, F) after vapothermal pre-treatment (top) and hydrothermal pre-treatment (bottom). Pre-treatment temperature: 150 °C. Error bars are not available for C, D, and F as no triple-determination was conducted.

temperature (Fig. 3A and D). Under milder conditions, mass loss was minimal for vapothermally pre-treated samples while it ranged from 9 to 13 $\%_{DM}$ for hydrothermal pre-treatment. The mass loss of the samples pre-treated at 170 °C differed by 14 %pt. (vapothermal 8 $\%_{DM}$, hydrothermal 22 $\%_{DM}$) and the difference was even greater at 190 °C. Overall, mass loss was consistently higher for hydrothermal pre-treatment.

Both pre-treatment options impacted the biomass molecular composition and structure in a similar way (Fig. 3B and E). Major effects can be summarized as follows: the cellulose content increased with pre-treatment temperature, especially after hydrothermal pre-treatment (+ 51 %; + 16 % for vapothermal, 190 °C). The hemicellulose content decreased with pre-treatment temperature, with close to complete solubilization and contents dropping below 6 wt–% (190 °C). The lignin content increased slightly with increasing temperature, reaching a maximum at 190 °C. Acetate was largely solubilized for both pre-treatments at 170 °C (solubilization ~ 30 to 40 %) and especially at 190 °C (solubilization ~ 70 %). Overall, during hydrothermal pre-treatment, the anaerobically degradable cellulose increased relative to the non-degradable lignin with increasing temperature. For the vapothermal pre-treatment, this was rather overcompensated by a relative increase of lignin.

The FTIR spectra (see supplementary material) of the samples treated at different temperatures varied across the measurement range, indicating compositional and structural changes. These effects are reflected in the *CR*, *LOI,* and *CR* (Fig. 3C and F). The *CR* tendentially decreased, while the *LOI* rather increased with pre-treatment temperature. The *CL* ratio decreased from 2.0 to as low as 1.2 after vapothermal pre-treatment and 1.1 after hydrothermal pre-treatment. This would usually indicate a decrease in cellulose compared to lignin. As this is not consistent with the compositional analysis, the change in the *CL* ratio is probably rather related to structural changes impacting the peak heights instead of actual compositional changes.

Residence time had minimal impact on mass loss in vapothermal pre-treatment, while hydrothermal pre-treatment caused over 10 % mass loss at all residence times (Fig. 4A and D). The compositional analysis (Fig. 4B and E) as well as the *CL* ratio did not show relevant changes caused by the variation of residence time (Fig. 4C and F). The FTIR spectra were very similar across the measurement range (see supplementary material), and the structural indices *CR* and *LOI* showed only small deviations or unclear trends (Fig. 4C and F).

The composition of the untreated common reed was in agreement with the literature (Baute et al., 2018), even though the lignin content of the samples assessed in this study was relatively high. Regarding the effect of pre-treatment temperature, higher temperatures typically result in increased hemicellulose degradation and solubilization after both vapothermal (Bauer et al., 2014) and hydrothermal pre-treatment (Varongchayakul et al., 2022). Essentially, xylose and arabinose are solubilized while other fractions are not liquefied to the same extent (Parsin and Kaltschmitt, 2024). In fact, hemicellulose solubilization over 90 % can be realized (hydrothermal pre-treatment, 200 °C / 15 min (Varongchayakul et al., 2022)). Due to the high acetate solubilization observed at 170 °C, further pH reduction at these temperatures, accompanied by an additional enhancement of autohydrolysis, can be assumed (Agbor et al., 2011; Mosier et al., 2005). Cellulose and lignin were largely retained in the solid biomass being a typical effect for vapothermal and hydrothermal pre-treatment (Parsin and Kaltschmitt, 2024; Reynolds et al., 2015). The difference in cellulose retention between the two pre-treatment methods could be explained by higher lignin solubilization during hydrothermal pre-treatment (Reynolds et al., 2015; Yelle et al., 2013), which generally leads to greater biomass solubilization (Funke et al., 2013), as reflected in the alleviated mass loss. This effect has also been observed by other studies related to vapothermal and hydrothermal pre-treatment (e.g., for wheat straw (Reynolds et al., 2015; Yelle et al., 2013)).

The FTIR spectra and derived indices suggested structural changes after pre-treatment. These changes have, for example, been documented in scanning electron microscope images taken after hydrothermal pre-treatment (López González and Heiermann, 2021; Varongchayakul et al., 2022). The *CR* decreased with pre-treatment severity (increasing temperature), indicating a reduction in crystallinity (Nelson and O'Connor, 1964). A moderate reduction in crystallinity at higher temperatures is commonly observed (Abbasi-Riyakhuni et al., 2025) and could be favorable for enhanced anaerobic degradability. The *LOI* increased with pre-treatment temperature. However, when considering the *LOI* alone, it is not always possible to differentiate whether the trend is caused by crystallinity changes or allomorphic changes (Lourdin et al., 2016). Considering the trend of the *CR*, it is likely that the increase of the index is related to a decrease in crystallinity of cellulose type II and/or an allomorphic transformation of cellulose type I to cellulose type II (Hurtubise and Krassig, 1960).

Regarding residence time, literature has documented its effect on hemicellulose solubilization for both methods (Bauer et al., 2014; Varongchayakul et al., 2022). An elongation of the residence time can be effective under circumstances, e.g., at low treatment temperatures (Abbasi-Riyakhuni et al., 2025). However, the current study suggests that the residence time is not a decisive factor within the tested temperature range.

3.2.2. Biogas and methane potential

Pre-treatment temperature affected biogas and methane potential in anaerobic digestion, with the highest yield at 170 °C for both methods (residence time 30 min). Precisely, the methane potential increased significantly from 192.7 ± 6.2 $mL_N\ CH_4\ g_{VS}^{-1}$ (original sample; biogas potential 276.9 ± 33.7 $mL_N\ g_{VS}^{-1}$) to 247.2 ± 9.6 $mL_N\ CH_4\ g_{VS}^{-1}$ (biogas potential 400.3 ± 14.4 $mL_N\ g_{VS}^{-1}$) after vapothermal pre-treatment, accounting for an increase of roughly 28 % methane (Fig. 5A and B). After hydrothermal pre-treatment, the methane yield increased by approximately 36 % to 263.1 ± 9.0 $mL_N\ CH_4\ g_{VS}^{-1}$ (biogas potential 410.8 ± 16.4 $mL_N\ g_{VS}^{-1}$, (Fig. 5E and F)). Even though the increase was slightly stronger for hydrothermal pre-treatment, the difference was not statistically significant. To account for the effect of digestible organic matter (predominantly hemicellulose) being solubilized from the solid organic matter during the pre-treatment, while non-digestible lignin accumulates, the biogas potential based on digestible organic dry mass (defined here as all organic mass excluding lignin) was evaluated as well (Fig. 5D and H). In both cases, a similar trend became obvious compared to the biogas potential based on organic dry mass, showing the optimum at 170 °C and a decreasing potential at 190 °C. When considering the mass loss, in the case of vapothermal pre-treatment, the increase in methane yield surpassed the mass loss of 8 % (section 3.2.1). Hence, the methane yield increased by 18 % instead of 28 % to 227.9 $mL_N\ CH_4\ g_{VS}^{-1}$ (vapothermal). However, in the case of hydrothermal pre-treatment, the mass loss of 22 % largely offset the increase. Accordingly, the methane yield increased to 205.2 $mL_N\ CH_4\ g_{VS}^{-1}$ which is an increase of 6 % instead of 36 %.

Both pre-treatments had the same temperature optimum, but their effects differed across the temperature range. Hydrothermal pre-treatment had a broader temperature optimum with an increase of biogas and methane potential across all pre-treatment temperatures. This effect was significant for the pre-treatment at 150 °C and 170 °C (Fig. 5E, F, G, and H). Vapothermal pre-treatment exhibited a narrow optimum (i.e., the impact was only significant at 170 °C; Fig. 5A, B, C, and D). This is interesting since the pre-test series and the model derived from it (section 3.1) were not able to predict this temperature optimum. Most likely the experimental conditions in the pre-test series failed to capture the narrow optimum, as no increase in biogas production was observed at 135 °C, 155 °C, and 180 °C.

The two pre-treatments affected the degradation kinetics differently (Table 6). The maximum biogas production rate (R_m) increased for all pre-treatment conditions. This effect was stronger for hydrothermal pre-treatment, consistent with the biogas and methane data. Further, the pre-treatment reduced the degradation lag phase. Compared to the

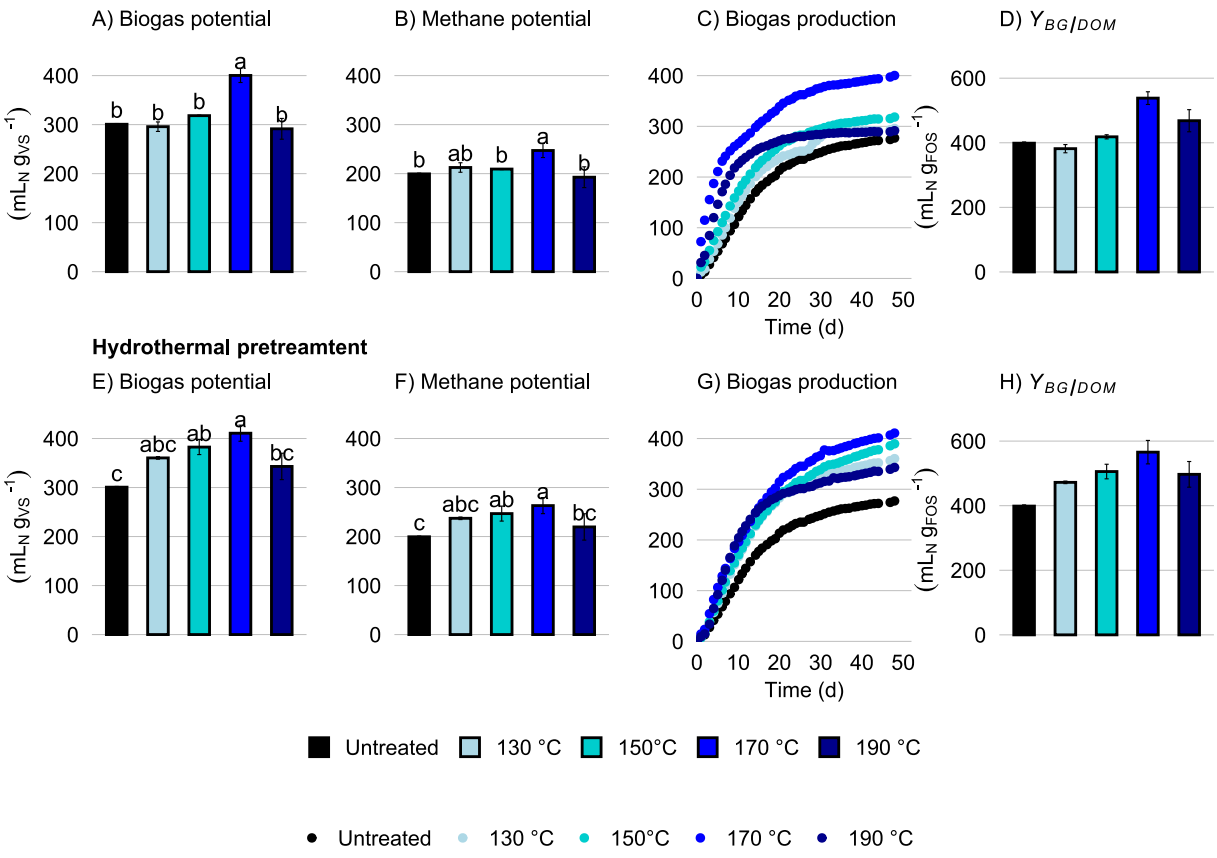

Fig. 5. Biogas potential (A, E, ($n = 3$)), methane potential (B, F, ($n = 3$)), biogas production over time (C, G, ($n = 3$)) and the biogas potential based on digestible organic dry mass ($Y_{BG/DOM}$) (D, H, ($n = 3$)) after vapothermal pre-treatment (top) and hydrothermal pre-treatment (bottom). Pre-treatment duration 30 min. Compact letter display (lowercase letters) indicates significant differences between samples ($p < 0.5$).

Table 6
Kinetic parameters of common reed after vapothermal and hydrothermal pre-treatment (main test series). T: Temperature, t: residence time.

Treatment			P ($mL_N\ g_{VS}^{-1}$)	R_m ($mL_N\ g_{VS}^{-1}\ d^{-1}$)	λ (d)	R^2 (−)	RMSE ($mL_N\ g_{VS}^{-1}$)
untreated			292.8	14.50	1.2	0.997	4.63
	T (°C)	t (min)					
Vapothermal	130	30	292.9	14.74	0.4	0.990	8.69
	150	10	305.7	15.97	0.2	0.996	5.62
	150	20	314.6	16.84	0.2	0.996	5.62
	150	30	310.5	15.98	−0.4	0.995	6.02
	170	30	385.2	19.82	−4.0	0.959	17.59
	190	30	283.4	25.47	−0.3	0.990	7.05
Hydrothermal	130	30	346.4	17.57	0.9	0.996	6.79
	150	10	342.5	15.45	0.4	0.993	8.77
	150	20	320.5	16.73	0.8	0.997	5.25
	150	30	373.2	16.66	0.5	0.993	9.35
	170	30	397.6	18.02	−0.3	0.993	9.87
	190	30	322.6	21.89	1.0	0.990	9.65

untreated sample, the lag phase (λ, Table 6) was shorter after hydrothermal pre-treatment and even shorter after vapothermal pre-treatment. These altered degradation kinetics are reflected in the biogas production over time shown in Fig. 5C and G. After vapothermal pre-treatment biogas production was shifted towards earlier time steps (smaller λ, higher R_m). It was more spread across time after hydrothermal pre-treatment, but still faster compared to the untreated sample.

A significant effect of the residence on biogas and methane production was not observed for any vapothermal sample (Fig. 6A, B, C, and D). This was already established in the pre-test series (30 and 90 min) and confirmed when shorter residence times (10 to 30 min) were applied. Since longer residence time showed no clear benefit, relatively short residence times are applicable, allowing higher throughput without compromising pre-treatment effectiveness. Contrastingly, a longer residence time proved beneficial in hydrothermal pre-treatment (Fig. 6E, F, G, and H), although the sample treated for 20 min was an exception.

Vapothermal pre-treatment using an optimized biomass water content, as determined in this study, resulted in a similar or higher increase in methane potential compared to other published investigations, which report increases in the range of 15 to 27 % (Bauer et al., 2014; Bauer et al., 2009; Ferreira et al., 2014; Ferreira et al., 2013). Even though there is evidence for the optimum conditions during vapothermal pre-treatment being rather narrow (Bauer et al., 2009), the pre-treatment temperature and residence time optima might differ greatly among publications. For instance, published optimal pre-treatment conditions

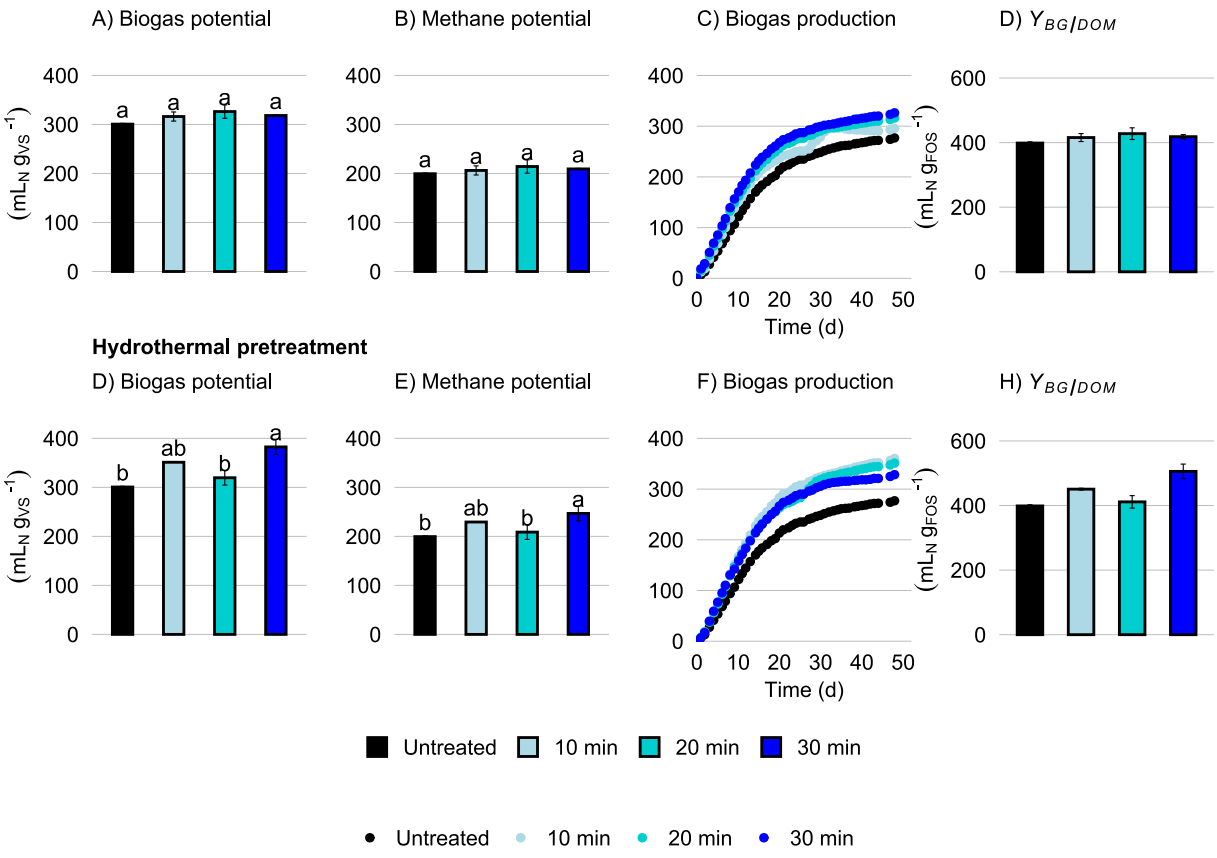

Fig. 6. Biogas potential (A, D, ($n = 3$)), methane potential (B, E, ($n = 3$)), biogas production over time (C, F, ($n = 3$)) and the biogas potential based on digestible organic dry mass ($Y_{BG/DOM}$) (D, H, ($n = 3$)) after vapothermal pre-treatment (top) and hydrothermal pre-treatment (bottom). Pre-treatment temperature 150 °C. Compact letter display (lowercase letters) indicates significant differences between samples ($p < 0.5$).

for wheat straw were 200 °C for 5 min (27 % increase in methane potential (Ferreira et al., 2014)), 200 °C for 1 min (20 % increase (Ferreira et al., 2013)), and 180 °C for 15 min (20 % increase (Bauer et al., 2009)). Steam explosion pre-treatment of hay resulted in a 16 % increase in methane potential at relatively harsh conditions (220 °C for 15 min (Bauer et al., 2014)). The failure of the Box-Behnken screening test in the pre-test series to predict the high biogas potential after pre-treatment at 170 °C highlights a key limitation. This issue may arise from excessively wide parameter ranges, failing to accurately identify the true optimum. Additionally, while the Box-Behnken design is efficient in terms of the number of experimental runs, it inherently lacks coverage at the corner points. Employing an alternative experimental design, such as a Central Composite Design, which includes axial points and better explores the parameter space, could mitigate these shortcomings and improve the identification of the true optimum (Heckert et al., 2002). This demonstrates that the identification of optimal conditions always depends on the specific design of the experiments.

Compared to published data (López González and Heiermann, 2021; Shang et al., 2019), the effectiveness of the hydrothermal pre-treatment (36 % increase in methane potential) was rather low (e.g., methane potentials were reported to increase by more than 60 % as a consequence of hydrothermal pre-treatment (López González and Heiermann, 2021; Shang et al., 2019)). At the same time, these publications reported similar temperature optima (180 °C and 175 °C) and comparable residence time ranges (20 min, 30 min (López González and Heiermann, 2021; Shang et al., 2019)). Nevertheless, the biogas increase measured in this study was still respectable, as other studies (Varongchayakul et al., 2022) reported lower increases in methane potential, ranging from 15 to 20 % (Varongchayakul et al., 2022). Differences among publications are often considerably influenced by the type of biomass used, also the particle size during treatment impacts the results, and such deviations are therefore understandable. Additionally, the observed changes in degradation kinetics, which shifted the biogas production more toward the beginning of the experiment, are consistent with literature (Varongchayakul et al., 2022).

Relating these findings to the compositional and structural changes presented above (section 3.2.1), an increased biogas production potential could be related to the retention of cellulose in the solid residues, a reduction in cellulose crystallinity, along with effects such as increased surface area due to hemicellulose solubilization. The success of the treatment is probably because an enlarged surface area in combination with increased pore volume improves enzyme permeability (Abbasi-Riyakhuni et al., 2025). However, there are also counteracting effects, that might compromise the success of the treatment, such as the loss of digestible organic mass, hemicellulose dissolution, and lignin accumulation. This might explain why the biogas potential was not significantly higher after the pre-treatments at 190 °C compared to the untreated substrate. However, based on only the digestible organic dry mass, the biogas potential decreased from 170 to 190 °C. Consequently, either the easily degradable organic matter was solubilized at temperatures higher than 170 °C and/or further effects reduced the biodegradability of the theoretically digestible organic components. The latter could be explained by either the formation of inhibiting substances like pseudo lignin from carbohydrates (Bauer et al., 2014; Sannigrahi et al., 2011) or by repolymerization reactions and lignin redeposition possibly leading to a reduced cellulose availability (Steinbrecher et al., 2022).

In summary, the temperature seemed to play a more decisive role than the residence time when treating the biomass with one of methods. The temperature optimum of the two applications was similar, even though the optimum for a vapothermal pre-treatment was much more difficult to capture and might differ from biomass to biomass – requiring optimization for the respective use case. Vapothermal pre-treatment was

less susceptible to mass loss. Further, results suggest that longer pre-treatment times were only beneficial for hydrothermal pre-treatment, while short residence times were sufficiently effective for vapothermal pre-treatment. The increase of the biogas and methane yield of common reed due to vapothermal or hydrothermal pre-treatment was related to the induced compositional and structural changes.

3.3. Energetic evaluation and systemic placement of findings

The process integration of hydrothermal pre-treatment is currently not considered economically feasible, with the costs being dominated in particular by the high energy costs (Ruiz et al., 2023). Pre-treatment based on vapor might offer substantial energy savings compared to a hydrothermal pre-treatment because it requires less water to be heated and it is effective at a much shorter residence time (Ferreira et al., 2013). This deduction is supported by the estimation of the energy demand of both methods. These estimations show that the energy demand of heating 1 kg of biomass (dry mass) and the required amount of pre-treatment medium to process temperature could be more than 10-fold higher for hydrothermal pre-treatment. The respective energy needed was estimated to be 640 kJ kg_{DM}^{-1} for vapothermal pre-treatment and 7,140 kJ kg_{DM}^{-1} for hydrothermal pre-treatment. This is related to the amount of energy required to heat the treatment medium (i.e., steam and water). While the energy required to provide (i.e., evaporation energy) and heat steam for vapothermal pre-treatment of 1 kg of dry biomass would be around 120 kJ kg_{DM}^{-1}, heating the bulk water to the process temperature would require 1,420 kJ kg_{DM}^{-1} for hydrothermal pre-treatment.

Looking beyond the applied system boundaries, the liquid fraction of hydrothermal pre-treated material as well as the liquid hydrolysate or condensate of vapothermal pre-treatment could be used for isolating high-value products like xylooligosaccharides (Parsin and Kaltschmitt, 2024). Moreover, the liquid hydrolysate may contain furfurals, as well as organic acids such as glycolic, formic and acetic acid (Li et al., 2013). Two prominent molecules among furfurals are the 6-C-atom molecule 5-hydroxymethylfurfural derived from hexoses (e.g., building blocks of cellulose) and the 5-C-atom molecule furfural derived from pentose (e.g., building blocks of hemicellulose) (Steinbach et al., 2017). These two molecules are considered among the most valuable platform chemicals, holding significant potential for a use within biorefineries (Bozell and Petersen, 2010). Alternatively, if applicable, the hydrolysate could be added as liquid phase to the biogas reactor, so the solubilized hemicellulose could be converted to biogas as well.

4. Conclusion

To facilitate anaerobic conversion of lignocellulosic biomass, biogas and methane potential of solid residues of vapothermal and hydrothermal pre-treatment were assessed.

Optimizing the water content during vapothermal pre-treatment via water impregnation of feedstock was beneficial for the success of the pre-treatment. Pre-treatment temperature significantly influenced the biomass composition, structure, and gas yields. The optimum for both methods was 170 °C, at which both methods yielded equal amounts of biogas. Taking the mass loss into consideration, vapothermal pre-treatment outcompeted hydrothermal pre-treatment. Also, a short residence time was sufficient to achieve the desired effect with vapothermal pre-treatment.

In conclusion, vapothermal pre-treatment with optimized initial water content of lignocellulosic biomass showed similar or better biogas and methane yields, with less time and energy required compared to hydrothermal pre-treatment. This suggests that it could be a more efficient, cost-effective option for large-scale implementation. Future research should validate these findings through techno-economic and ecological assessments.

CRediT authorship contribution statement

Jana Schultz: Conceptualization, Methodology, Software, Formal analysis, Investigation, Writing – original draft, Visualization. **Marvin Scherzinger:** Conceptualization, Methodology, Formal analysis, Writing – review & editing. **Timo Steinbrecher:** Conceptualization, Investigation, Formal analysis, Writing – review & editing. **Asli Isci:** Methodology, Investigation, Writing – review & editing. **Martin Kaltschmitt:** Resources, Writing – review & editing, Supervision, Project administration, Funding acquisition.

Declaration of competing interest

The authors declare the following financial interests/personal relationships which may be considered as potential competing interests: Jana Schultz reports financial support was provided by German Federal Ministry of Education and Research. Martin Kaltschmitt, Marvin Scherzinger, Timo Steinbrecher reports financial support was provided by German Federal Ministry of Education and Research. Asli Isci reports financial support was provided by Scientific and Technological Research Council of Turkey. If there are other authors, they declare that they have no known competing financial interests or personal relationships that could have appeared to influence the work reported in this paper.

Acknowledgements

This research is part of the international research project ReMediation (Resilient Mediterranean with a holistic approach to sustainable agriculture: Addressing challenges of water, soil, energy and biodiversity; https://remediationproject.com/) within the PRIMA program (https://prima-med.org/). The authors acknowledge the financial support for the work published by the German Federal Ministry of Education and Research (grant number: 02WPM1656) and The Scientific and Technological Research Council of Turkey (TÜBİTAK) (Project No: 122N048).

Appendix A. Supplementary data

Supplementary data to this article can be found online at https://doi.org/10.1016/j.biortech.2025.132329.

Data availability

Data will be made available on request.

References

Abbasi-Riyakhuni, M., Hashemi, S.S., Denayer, J.F., Aghbashlo, M., Tabatabaei, M., Karimi, K., 2025. Integrated biorefining of rapeseed straw for ethanol, biogas, and mycoprotein production. Fuel 382, 133751. https://doi.org/10.1016/j.fuel.2024.133751.

Agbor, V.B., Cicek, N., Sparling, R., Berlin, A., Levin, D.B., 2011. Biomass pretreatment: fundamentals toward application. Biotechnology Advances 29, 675–685. https://doi.org/10.1016/j.biotechadv.2011.05.005.

Baksi, S., Saha, D., Saha, S., Sarkar, U., Basu, D., Kuniyal, J.C., 2023. Pre-treatment of lignocellulosic biomass: review of various physico-chemical and biological methods influencing the extent of biomass depolymerization. Int. J. Environ. Sci. Technol. 20, 13895–13922. https://doi.org/10.1007/s13762-023-04838-4.

Bauer, A., Bösch, P., Friedl, A., Amon, T., 2009. Analysis of methane potentials of steam-exploded wheat straw and estimation of energy yields of combined ethanol and methane production. Journal of Biotechnology 142, 50–55. https://doi.org/10.1016/j.jbiotec.2009.01.017.

Bauer, A., Lizasoain, J., Theuretzbacher, F., Agger, J.W., Rincón, M., Menardo, S., Saylor, M.K., Enguídanos, R., Nielsen, P.J., Potthast, A., Zweckmair, T., Gronauer, A., Horn, S.J., 2014. Steam explosion pretreatment for enhancing biogas production of late harvested hay. Bioresour. Technol. 166, 403–410. https://doi.org/10.1016/j.biortech.2014.05.025.

Baute, K., van Eerd, L.L., Robinson, D.E., Sikkema, P.H., Mushtaq, M., Gilroyed, B.H., 2018. Comparing the Biomass Yield and Biogas Potential of Phragmites australis with Miscanthus x giganteus and Panicum virgatum Grown in Canada. Energies 11, 2198. https://doi.org/10.3390/en11092198.

Bisaria, V., 2024. Handbook of Biorefinery Research and Technology: Biomass Logistics to Saccharification. Springer, Netherlands, Dordrecht.
Bozell, J.J., Petersen, G.R., 2010. Technology development for the production of biobased products from biorefinery carbohydrates—the US Department of Energy's "Top 10" revisited. Green Chem. 12, 539. https://doi.org/10.1039/B922014C.
Buratti, C., Barbanera, M., Lascaro, E., Cotana, F., 2018. Optimization of torrefaction conditions of coffee industry residues using desirability function approach. Waste Management (new York N.Y.) 73, 523–534. https://doi.org/10.1016/j.wasman.2017.04.012.
Deutsches Institut für Normung e. V., 2012. DIN EN 15935. Sludge, treated biowaste, soil and waste - Sludge, Sludge, treated biowaste, soil and waste - Determination of loss on ignition loss on ignition. Deutsches Institut für Normung e. V.
Deutsches Institut für Normung e. V., 2015. DIN EN ISO 18134. Solid biofuels – Determination of moisture content. Deutsches Institut für Normung e. V.
Ferreira, L.C., Donoso-Bravo, A., Nilsen, P.J., Fdz-Polanco, F., Pérez-Elvira, S.I., 2013. Influence of thermal pretreatment on the biochemical methane potential of wheat straw. Bioresour. Technol. 143, 251–257. https://doi.org/10.1016/j.biortech.2013.05.065.
Ferreira, L.C., Nilsen, P.J., Fdz-Polanco, F., Pérez-Elvira, S.I., 2014. Biomethane potential of wheat straw: Influence of particle size, water impregnation and thermal hydrolysis. Chemical Engineering Journal 242, 254–259. https://doi.org/10.1016/j.cej.2013.08.041.
FNR, n.d. Schilfrohr. Fachagentur Nachwachsende Rohstoffe e.V. https://baustoffe.fnr.de/daemmstoffe/materialien/schilfrohr (accessed 30 October 2024).
Funke, A., Reebs, F., Kruse, A., 2013. Experimental comparison of hydrothermal and vapothermal carbonization. Fuel Processing Technology 115, 261–269. https://doi.org/10.1016/j.fuproc.2013.04.020.
Heckert, N., Filliben, J., Croarkin, C., Hembree, B., Guthrie, W., Tobias, P., Prinz, J., 2002. Handbook 151: NIST/SEMATECH e-Handbook of Statistical Methods: NIST Interagency/Internal Report (NISTIR). Gaithersburg, MD.
Hurtubise, F.G., Krassig, H., 1960. Classification of Fine Structural Characteristics in Cellulose by Infared Spectroscopy. Use of Potassium Bromide Pellet Technique. Analytical Chemistry 32, 177–181.
Iea, 2020. Outlook for biogas and biomethane: Prospects for organic growth, 93 pp. accessed 25 October 2023. https://iea.blob.core.windows.net/assets/03aeb10c-c38c-4d10-bcec-de92e9ab815f/Outlook_for_biogas_and_biomethane.pdf.
Li, H.-Q., Li, C.-L., Sang, T., Xu, J., 2013. Pretreatment on Miscanthus lutarioriparious by liquid hot water for efficient ethanol production. Biotechnology for Biofuels 6, 76. https://doi.org/10.1186/1754-6834-6-76.
Lizasoain, J., Rincón, M., Theuretzbacher, F., Enguídanos, R., Nielsen, P.J., Potthast, A., Zweckmair, T., Gronauer, A., Bauer, A., 2016. Biogas production from reed biomass: Effect of pretreatment using different steam explosion conditions. Biomass and Bioenergy 95, 84–91. https://doi.org/10.1016/j.biombioe.2016.09.021.
López González, L.M., Heiermann, M., 2021. Effect of Liquid Hot Water Pretreatment on Hydrolysates Composition and Methane Yield of Rice Processing Residue. Energies 14, 3254. https://doi.org/10.3390/en14113254.
Lourdin, D., Peixinho, J., Bréard, J., Cathala, B., Leroy, E., Duchemin, B., 2016. Concentration driven cocrystallisation and percolation in all-cellulose nanocomposites. Cellulose 23, 529–543. https://doi.org/10.1007/s10570-015-0805-x.
Lynam, J.G., Kumar, N., Wong, M.J., 2017. Deep eutectic solvents' ability to solubilize lignin, cellulose, and hemicellulose; thermal stability; and density. Bioresour. Technol. 238, 684–689. https://doi.org/10.1016/j.biortech.2017.04.079.
Lynd, L.R., Weimer, P.J., van Zyl, W.H., Pretorius, I.S., 2002. Microbial cellulose utilization: fundamentals and biotechnology. Microbiology and molecular biology reviews : MMBR 66, 506-77, table of contents. https://doi.org/10.1128/mmbr.66.3.506-577.2002.
Mosier, N., Wyman, C., Dale, B., Elander, R., Lee, Y.Y., Holtzapple, M., Ladisch, M., 2005. Features of promising technologies for pretreatment of lignocellulosic biomass. Bioresour. Technol. 96, 673–686. https://doi.org/10.1016/j.biortech.2004.06.025.
Nelson, M.L., O'Connor, R.T., 1964. Relation of Certain Intrared Bands to Cellulose Crystallinity and Crystal Lattice Type. part II. A New Infrared Ratio for Estimation of Crystallinity in Cellulose I and II. J. Appl. Polym. Sci. 8, 1325–1341.
Olsson, L. (Ed.), 2007. Biofuels. Springer, Berlin, Heidelberg, New York, p. 368.
Parsin, S., Kaltschmitt, M., 2024. Processing of hemicellulose in wheat straw by steaming and ultrafiltration - A novel approach. Bioresour. Technol. 393, 130071. https://doi.org/10.1016/j.biortech.2023.130071.
Perez-Cantu, L., Schreiber, A., Schütt, F., Saake, B., Kirsch, C., Smirnova, I., 2013. Comparison of pretreatment methods for rye straw in the second generation biorefinery: effect on cellulose, hemicellulose and lignin recovery. Bioresour. Technol. 142, 428–435. https://doi.org/10.1016/j.biortech.2013.05.054.
Pitard, F.F., 1993. Pierre Gy's sampling theory and sampling practice: Heterogeneity, sampling correctness, and statistical process control, 2nd ed. CRC Press, Boca Raton, Fla., p. 488
Reynolds, W., Kirsch, C., Smirnova, I., 2015. Thermal-Enzymatic Hydrolysis of Wheat Straw in a Single High Pressure Fixed Bed. Chemie Ingenieur Technik 87, 1305–1312. https://doi.org/10.1002/cite.201400192.
Roj-Rojewski, S., Wysocka-Czubaszek, A., Czubaszek, R., Kamocki, A., Banaszuk, P., 2019. Anaerobic digestion of wetland biomass from conservation management for biogas production. Biomass and Bioenergy 122, 126–132. https://doi.org/10.1016/j.biombioe.2019.01.038.
Ruiz, H.A., Sganzerla, W.G., Larnaudie, V., Veersma, R.J., van Erven, G., Shiva, R.-G., L. J., Rodríguez-Jasso, R.M., Rosero-Chasoy, G., Ferrari, M.D., Kabel, M.A., Forster-Carneiro, T., Lareo, C.,, 2023. Advances in process design, techno-economic assessment and environmental aspects for hydrothermal pretreatment in the fractionation of biomass under biorefinery concept. Bioresource Technology 369, 128469. https://doi.org/10.1016/j.biortech.2022.128469.
Sannigrahi, P., Kim, D.H., Jung, S., Ragauskas, A., 2011. Pseudo-lignin and pretreatment chemistry. Energy Environ. Sci. 4, 1306–1310. https://doi.org/10.1039/C0EE00378F.
Scherzinger, M., Kulbeik, T., Kaltschmitt, M., 2020. Autoclave pre-treatment of green wastes – Effects of temperature, residence time and rotation speed on fuel properties. Fuel 273, 117796. https://doi.org/10.1016/j.fuel.2020.117796.
Shang, G., Zhang, C., Wang, F., Qiu, L., Guo, X., Xu, F., 2019. Liquid hot water pretreatment to enhance the anaerobic digestion of wheat straw-effects of temperature and retention time. Environmental Science and Pollution Research International 26, 29424–29434. https://doi.org/10.1007/s11356-019-06111-z.
Shi, J., Li, J., 2012. Metabolites and chemical changes in the wood-forming tissue of pinus koraiensis under inclined conditions. BioResources 7, 3463–3475.
Siebertz, K., van Bebber, D., Hochkirchen, T., 2017. Statistische Versuchsplanung: Design of Experiments (DoE), 2nd ed. Springer Vieweg, Berlin, Heidelberg, p. 508.
Sluiter, A., Hames, B., Ruiz, R., Scarlata, C., Sluiter, J., Templeton, D., Crocker, D., 2008. Determination of Structural Carbohydrates and Lignin in Biomass: Laboratory Analytical procedure (LAP). NREL/TP-510-42618. National Renewable Energy Laboratory.
Steinbach, D., Kruse, A., Sauer, J., 2017. Pretreatment technologies of lignocellulosic biomass in water in view of furfural and 5-hydroxymethylfurfural production- A review. Biomass Conv. Bioref. 7, 247–274. https://doi.org/10.1007/s13399-017-0243-0.
Steinbrecher, T., Bonk, F., Scherzinger, M., Lüdtke, O., Kaltschmitt, M., 2022. Fractionation of Lignocellulosic Fibrous Straw Digestate by Combined Hydrothermal and Enzymatic Treatment. Energies 15, 6111. https://doi.org/10.3390/en15176111.
Sui, W., Chen, H., 2015. Water transfer in steam explosion process of corn stalk. Industrial Crops and Products 76, 977–986. https://doi.org/10.1016/j.indcrop.2015.08.001.
Sui, W., Chen, H., 2016. Effects of water states on steam explosion of lignocellulosic biomass. Bioresour. Technol. 199, 155–163. https://doi.org/10.1016/j.biortech.2015.09.001.
Varongchayakul, S., Tinrung, N., Lerdlattaporn, R., Songkasiri, W., Chaiprasert, P., 2022. Evaluation of methane production from liquid hot water pretreated Paspalum atratum and Brachiaria ruziziensis as alternative energy substrates. Industrial Crops and Products 180, 114784. https://doi.org/10.1016/j.indcrop.2022.114784.
Velázquez-Martí, B., Meneses-Quelal, O.W., Gaibor-Chavez, J., Niño-Ruiz, Z., 2019. Review of Mathematical Models for the Anaerobic Digestion Process. In: Rajesh Banu, J. (Ed.), Anaerobic Digestion. IntechOpen.
Verein Deutscher Ingenieure, 2016. VDI 4630. Fermentation of organic materials - Characterisation of the substrate, sampling, collection of material data, fermentation tests. Beuth, Berlin 13.030.30, 27.190.
Wang, J., Ma, D., Lou, Y., Ma, J., Xing, D., 2023. Optimization of biogas production from straw wastes by different pretreatments: Progress, challenges, and prospects. The Science of the Total Environment 905, 166992. https://doi.org/10.1016/j.scitotenv.2023.166992.
Wang, J., Yue, Z.-B., Chen, T.-H., Peng, S.-C., Yu, H.-Q., Chen, H.-Z., 2010. Anaerobic digestibility and fiber composition of bulrush in response to steam explosion. Bioresour. Technol. 101, 6610–6614. https://doi.org/10.1016/j.biortech.2010.03.086.
Yelle, D.J., Kaparaju, P., Hunt, C.G., Hirth, K., Kim, H., Ralph, J., Felby, C., 2013. Two-Dimensional NMR Evidence for Cleavage of Lignin and Xylan Substituents in Wheat Straw Through Hydrothermal Pretreatment and Enzymatic Hydrolysis. Bioenerg. Res. 6, 211–221. https://doi.org/10.1007/s12155-012-9247-6.
Ziegler-Devin, I., Chrusciel, L., Brosse, N., 2021. Steam Explosion Pretreatment of Lignocellulosic Biomass: A Mini-Review of Theorical and Experimental Approaches. Frontiers in Chemistry 9, 705358. https://doi.org/10.3389/fchem.2021.705358.